Journal of Power Sources 217 (2012) 479–484

Contents lists available at SciVerse ScienceDirect

Journal of Power Sources

journal homepage: www.elsevier.com/locate/jpowsour

Short communication

Charge–discharge behavior of tin negative electrode for a sodium secondary battery using intermediate temperature ionic liquid sodium bis(fluorosulfonyl) amide–potassium bis(fluorosulfonyl)amide

Takayuki Yamamoto [a], Toshiyuki Nohira [a,*], Rika Hagiwara [a,*], Atsushi Fukunaga [a,b], Shoichiro Sakai [b], Koji Nitta [b], Shinji Inazawa [b]

[a] Graduate School of Energy Science, Kyoto University, Yoshida-honmachi, Sakyo-ku, Kyoto 606-8501, Japan
[b] Sumitomo Electric Industries Ltd., 1-1-3 Shimaya, Konohana-ku, Osaka 554-0024, Japan

HIGHLIGHTS

- ► Charge–discharge of Sn negative electrode was tested in Na/NaFSA–KFSA/Sn at 363 K.
- ► Three potential plateaus appeared during both charge and discharge cycles.
- ► 1st cycle charge and discharge capacities were 790 and 729 mA h $(g\text{-Sn})^{-1}$.
- ► Cycleability and capacity dropped due to volume change during alloying/de-alloying.
- ► Reversible capacity was 300 mA h $(g\text{-Sn})^{-1}$ for 15 cycles with most negative plateau.

ARTICLE INFO

Article history:
Received 4 April 2012
Accepted 29 May 2012
Available online 19 June 2012

Keywords:
Sodium secondary battery
Intermediate temperature
Ionic liquid
Bis(fluorosulfonyl)amide
Tin negative electrode
Cycleability

ABSTRACT

The charge–discharge behavior of a Sn negative electrode for use in a sodium secondary battery was investigated in an intermediate temperature ionic liquid, NaFSA–KFSA (x_{NaFSA} = 0.56, x_{KFSA} = 0.44, FSA = bis(fluorosulfonyl)amides), at 363 K. A Na/Sn half-cell was prepared using a Sn-film (10–12 μm[t]) electrode. The charge–discharge curves at 0.619 mA cm^{-2} with cut-off voltages of 0.005 and 1.200 V exhibited three potential plateaus in both the charging (alloying) and discharging (de-alloying) processes, indicating the formation of various alloy phases. Charge and discharge capacities as high as 790 and 729 mA h $(g\text{-Sn})^{-1}$, respectively, were obtained for the 1st cycle; however, the capacities decreased rapidly due to volume change during the alloying and de-alloying processes. The best cycleability was achieved when the lower and higher cut-off voltages were set to 0.005 and 0.200 V, respectively. In this case, a reversible capacity of about 300 mA h $(g\text{-Sn})^{-1}$ was obtained for the initial 15 cycles.

1. Introduction

Lithium ion batteries are widely used for mobile devices such as laptop computers and mobile phones. The prospective use of these batteries in large-scale applications such as electric vehicles and renewable energy storage is expected to fuel increased demand for lithium metal. However, recoverable reserves of lithium for mass production of large batteries are limited and are unevenly distributed in the world. Thus, a rise in the price of lithium is anticipated. Consequently, sodium secondary batteries have emerged as possible alternatives to Li-based counterparts owing to the abundance and practically negative standard redox potential of sodium [1–14]. Previous and current studies on sodium secondary batteries fall into two classifications according to the operation temperature. The first includes those operating at high temperatures of around 573 K such as Na/S [1,2] and Na/$NiCl_2$ [3,4] batteries. Although these batteries are characterized by higher electrode reaction rates, they require heating systems as well as heat insulators to maintain the operation temperature, which leads to an increase in the size and weight of the batteries. Moreover, energy consumption by the heaters decreases the energy density of the total battery system. There is also a potential risk posed by electrical short circuit if the mechanically fragile β″-alumina breaks during operation due to the high reactivity of liquefied sodium metal in this temperature range. The second class of sodium secondary batteries includes those operating at room temperature using

* Corresponding authors. Tel.: +81 75 753 5822; fax: +81 75 753 5906.
E-mail addresses: nohira@energy.kyoto-u.ac.jp (T. Nohira), hagiwara@energy.kyoto-u.jp (R. Hagiwara).

0378-7753/$ – see front matter © 2012 Elsevier B.V. All rights reserved.
http://dx.doi.org/10.1016/j.jpowsour.2012.05.110

organic solvents as electrolytes [5–14]. Due to the lower operating temperature, handling is much easier, heaters are not necessary, and a variety of component materials are available. However, there are safety issues due to the flammability and volatility of the organic solvents used for the electrolytes when the batteries are scaled up.

To circumvent these issues, we have been exploring a new class of molten salts or ionic liquids that have wide electrochemical windows and posses the capacity for reversible electrodepositon of metallic sodium. We have previously investigated the thermal properties of single salts, binary and ternary mixtures of alkali metal bis(trifluoromethylsulfonyl)amides (MTFSAs; M = Li, Na, K, Rb, Cs; TFSA = bis(trifluoromethylsulfonyl)amide) [15,16], and alkali bis(fluorosulfonyl)amides (MFSAs; M = Li, Na, K, Rb, Cs; FSA = bis(fluorosulfonyl)amide) [17,18]. In the case of the TFSA salts, it was found that a Na/$NaCrO_2$ battery utilizing the NaTFSA-CsTFSA melt exhibited excellent cycle and rate performance at 423 K [19]. Depending on the application conditions, however, lower operation temperatures are generally preferable. MFSA salts have melting points in the range of 370–410 K, and binary or ternary mixtures of MFSA exhibit lower melting temperatures than those of the single salts. For instance, the NaFSA–KFSA eutectic salt ($x_{NaFSA} = 0.56$, $x_{KFSA} = 0.44$) melts at 334 K [18]; the melt exhibits a wide electrochemical window of approximately 5 V as well as the capacity for sodium metal deposition/dissolution [17,20]. This intermediate temperature ionic liquid (ITIL) is unique since it consists entirely of inorganic ions. The viscosity, ionic conductivity, and density of this ITIL at 333–398 K are documented in our previous report [20], in which it was also reported that the $NaCrO_2$ positive electrode exhibits good cycleability over 100 cycles in this ITIL at 353 K. In the current study, sodium metal is used as a negative electrode, in which the potential issue of dendritic deposition is a recognized limitation. This highlights the need for development of more stable and safer negative electrode materials in general and for sodium secondary batteries in particular, to facilitate practical application.

Thus far, hard carbon [21], $NaTi_2(PO_4)_3$ [22], and $Na_2Ti_3O_7$ [23] have been studied as negative electrode materials for sodium secondary batteries, whereas in the case of lithium ion batteries, a number of alloy negative electrodes (Sn, Si, etc.) have been evaluated [24–26] with comparatively few reports on alloy negative electrodes for sodium secondary batteries [27]. Based on the phase diagram of the Sn–Na system [28], tin forms eight intermetallic compounds with sodium at 363 K. Thus, tin is a potential candidate for a negative electrode possessing a high theoretical capacity of 847 mA h $(g\text{-Sn})^{-1}$ for the most sodium-rich phase ($Na_{15}Sn_4$).

In this study, the charge–discharge characteristics of a Sn negative electrode were investigated in NaFSA–KFSA ITIL at 363 K. A Na/Sn half-cell was constructed using a Sn-film electrode with a thickness of 10–12 μm. The cycleability and capacity of the electrode were evaluated using several cut-off voltages.

2. Experimental

NaFSA and KFSA (Mitsubishi Materials Electronic Chemicals Co., Ltd.) were used to prepare the electrolyte. The salts were dried under vacuum at 353 K (NaFSA) or 333 K (KFSA) for 48 h prior to use. The NaFSA–KFSA eutectic salt (mol% NaFSA:KFSA = 56:44) was prepared by grinding the two salts in a mortar.

Electrochemical measurements were performed under Ar atmosphere using VSP electrochemical measurement apparatus (a Bio-Logic Co.). Cyclic voltammetry (CV) measurements were conducted using a three-electrode system. Sn film on Al foil or an Al plate (99.999%, Nilaco) were used as working electrodes. Sn film was electrodeposited on Al foil, which was used as a current collector. The thickness of the Sn film was estimated to be 10–12 μm based on the amount of Sn, which was determined by inductively coupled plasma mass spectrometry (ICP-MS) measurements. Both the reference and counter electrodes were made of Na metal (99.85%, Sigma–Aldrich, Inc.). The three-electrode beaker cell was heated using a mantle heater, and the temperature of the cell was monitored by a thermocouple and maintained at 363 K. Cyclic voltammograms were collected at a scan rate of 0.1 mV s^{-1} using the Sn-film electrode and 10 mV s^{-1} for the Al plate electrode.

Galvanostatic charge–discharge tests were performed using a two-electrode cell (Tomcell Japan Co., Ltd.). Sn film on Al foil and a Na plate were used as the electrodes. A glass fiber filter paper (Whatman, GF-A, 260 μm^t) was used as a separator. The separator was vacuum-impregnated with the electrolyte prior to the test. The current density was fixed at 0.619 mA cm^{-2}, which corresponds to the C/10 rate for the 10 μm^t Sn film. The operating temperature was 363 K for all of the tests in the present study. The cell was heated by a mantle heater, and the cell temperature was monitored by a thermocouple and maintained at 363 K.

3. Results and discussion

Based on the phase diagram of the Sn–Na system [28] shown in Fig. 1, there are eight intermetallic compounds at 363 K: $Na_{15}Sn_4$, Na_3Sn, Na_9Sn_4, NaSn, $NaSn_2$, $NaSn_3$, $NaSn_4$, and $NaSn_6$. It is anticipated that these Sn–Na alloys should be formed electrochemically.

Fig. 2 shows cyclic voltammograms for Al plate and Sn-film electrodes in NaFSA–KFSA at 363 K. The sweep directions are indicated by arrows in the figure. No prominent current is detected between 0 and 2.0 V vs. Na/Na^+ for the Al plate electrode. In contrast, steep increases of the cathodic currents are observed at 0.5 V, 0.3 V, and 0.1 V vs. Na/Na^+ for the Sn-film electrode. In the sweep to positive potential, a large anodic current peak is observed around 0.9 V. These cathodic and anodic currents are ascribed to the formation of a Sn–Na alloy and dissolution of Na from the alloy.

Charge–discharge curves of the Na/NaFSA–KFSA/Sn cell at 363 K with cut-off voltages of 0.005 and 1.200 V (Test No. 1) are shown in Fig. 3a. The charge (alloying) and discharge (de-alloying) capacities for the 1st cycle are 790 and 729 mA h $(g\text{-Sn})^{-1}$, corresponding to 93% and 86% of the theoretical capacity, respectively. Three potential plateaus are observed in both the charge and discharge curves, which presumably correspond to the coexisting

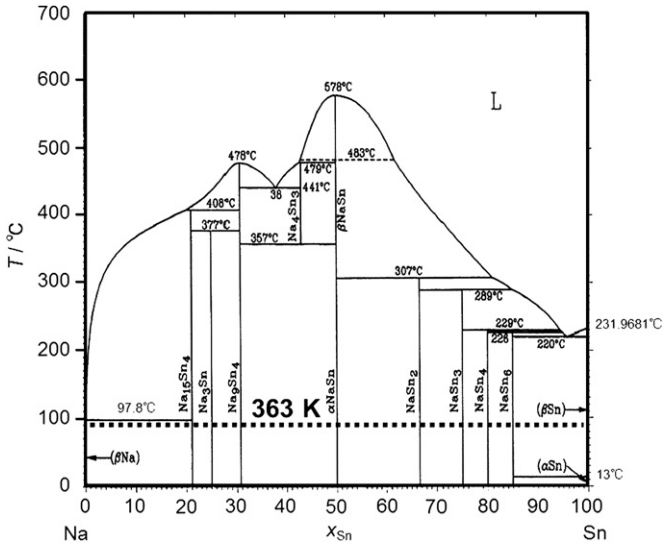

Fig. 1. Binary phase diagram for Sn–Na system.

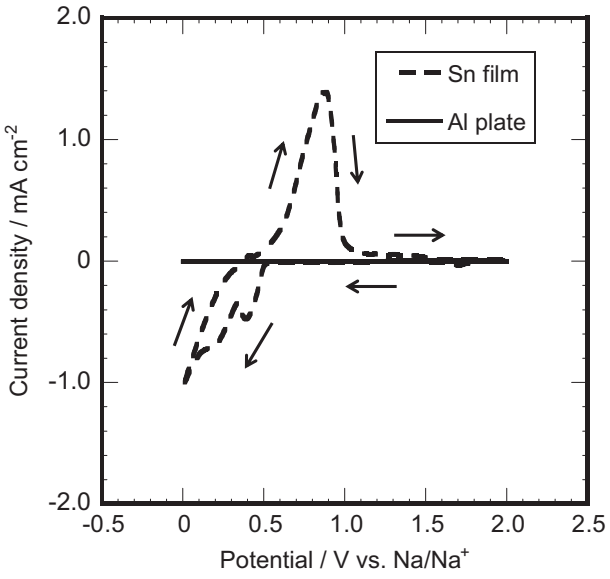

Fig. 2. Cyclic voltammograms for Sn-film and Al plate electrodes in NaFSA–KFSA at 363 K. Counter and reference electrodes: Na metal. Scan rate: 0.1 mV s^{-1}(Sn film) and 10 mV s^{-1}(Al plate).

phase states of Sn–Na alloys. The plateau potentials occur at: (a) 0.26 V, (b) 0.10 V, and (c) 0.04 V for the charge, and (a') 0.57 V, (b') 0.22 V, and (c') 0.12 V for the discharge process. Plateaus (a), (b), and (c) in the charge process may be associated with the same coexisting phase states (a'), (b'), and (c'), respectively, in the discharge process. However, based on the phase diagram, there is the possibility that several other potential plateaus may appear. In addition, there are relatively large potential differences between the plateaus in the charge process and those in the discharge process, especially between plateau (a) and (a'). Thus, more-detailed analysis is required to confirm the precise correlation between the plateaus in the charge and discharge process. Fig. 3b shows the specific capacities and coulombic efficiency versus the cycle number for 30 cycles. A high discharge capacity of ca. 700 mA h (g-Sn)$^{-1}$ was maintained during the initial three cycles. However, the capacity decreased rapidly to 204 mA h (g-Sn)$^{-1}$ in the 5th cycle and further to 121 mA h (g-Sn)$^{-1}$ in the 10th cycle. The coulombic efficiency of 92% in the 1st cycle decreased to 52% in the 5th cycle and remained a low value as 74% in 10th cycle. This decrease in the capacity and coulombic efficiency are indicative of deterioration of the electrode presumably because of the volume change during the alloying and de-alloying process, as is often observed for the Sn–Li system [26].

Here, the volume change of the electrode is estimated during the 1st discharge in Fig. 3a. The capacities corresponding to plateaus (a'), (b'), and (c') occur at approximately 200, 250, and 300 mA h (g-Sn)$^{-1}$, respectively. Table 1 lists the Sn–Na alloy phases reported in the phase diagram, the theoretical specific capacities, and the calculated molar volumes. Comparison of the experimentally observed capacities with the theoretical values leads to the following assignments as the most rational. Plateau (a') corresponds to NaSn (226 mA h (g-Sn)$^{-1}$) transforming into Sn. Similarly, plateau (b') corresponds to Na_9Sn_4 (508 mA h (g-Sn)$^{-1}$) changing into NaSn, with a theoretical capacity of 282 mA h (g-Sn)$^{-1}$, and plateau (c') corresponds to $Na_{15}Sn_4$ (847 mA h (g-Sn)$^{-1}$) converting into Na_9Sn_4, which theoretically corresponds to 339 mA h (g-Sn)$^{-1}$. The calculated values of the corresponding ratios of the volume contraction for each plateau were as follows: (a') 0.45 (=16.29/35.81), (b') 0.63 (=35.81/56.74), and (c') 0.66 (=56.74/85.34). Incidentally, when the fully charged alloy, $Na_{15}Sn_4$, is completely discharged, the volume contraction ratio becomes as small as 0.19 (=16.29/85.34). It was hypothesized that if electrode deterioration occurs mainly by the volume change, a charge–discharge test utilizing only one plateau should give better cycleability. Moreover, considering the contraction ratio, plateau (c) is expected to show the best cycleability.

In order to confirm the hypothesis stated above, three additional charge–discharge tests (Test Nos. 2–4, Table 2) were performed by changing the cut-off voltages. The detailed experimental conditions are summarized in Table 2. Fig. 4a shows the charge–discharge curves when the cut-off voltages were set to 0.200 and 1.200 V (Test No.2). In the first charge, plateau (a) is observed around 0.25 V and the charge capacity is 90 mA h (g-Sn)$^{-1}$. Increasing the cycle number results in the appearance of a new plateau (x) at around 0.45 V and the charge capacity increases to ca. 167 mA h (g-Sn)$^{-1}$ at the 10th cycle. Because the plateau potentials of (x) and (a') are close each other, it is plausible that they are ascribed to the coexistence of the same phases. In order to evaluate the correlation between the charge and discharge plateaus, however, a more detailed investigation, including phase identification by XRD, will be necessary. Fig. 4b shows the change in the specific capacity and coulombic efficiency with the cycle number. From the initial cycle

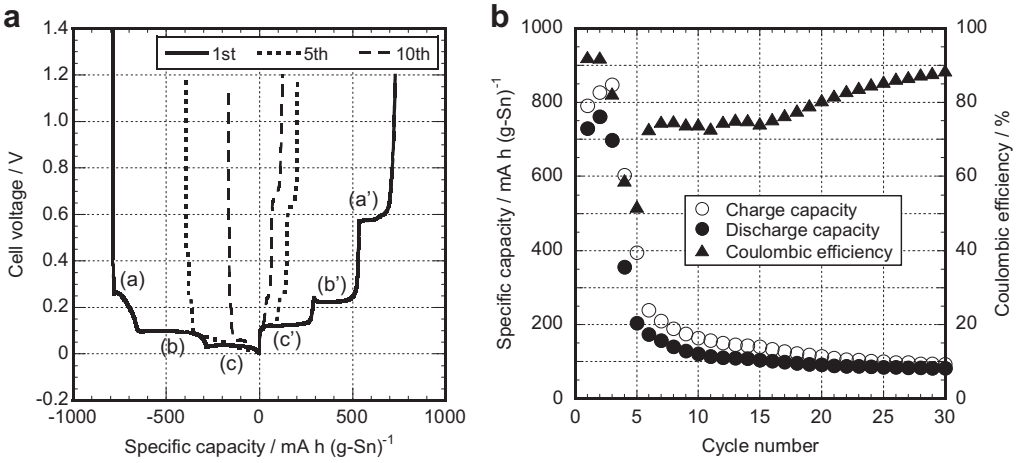

Fig. 3. (a) Charge–discharge curves and (b) cycling properties of specific capacity and coulombic efficiency of the Na/NaFSA–KFSA/Sn cell at 363 K. Cut-off voltages: 0.005 and 1.200 V. Current density: 0.619 mA cm^{-2}.

Table 1
Theoretical capacity and molar volume of Sn–Na alloy phases.

Phases	Capacity/ mA h (g-Sn)$^{-1}$	Molar volume/ cm^3 (mol-Sn)$^{-1}$
Sn	0	16.29 [28]
$NaSn_6$	37.6	N/A[a]
$NaSn_4$	56.4	N/A[a]
$NaSn_3$	75.3	N/A[a]
$NaSn_2$	113	26.12 [29]
NaSn	226	35.81 [30]
Na_9Sn_4	508	56.74 [31]
Na_3Sn	677	N/A[a]
$Na_{15}Sn_4$	847	85.34 [31]

[a] Crystal structure has not been reported.

Table 2
Conditions of charge–discharge tests.

Test No.	Plateaus	Cut-off voltages
1	(a), (b), and (c)	0.005 and 1.200 V
2	(a)	0.200 and 1.200 V
3	(b)	0.075 and 0.300 V
4	(c)	0.005 and 0.200 V

until the 9th cycle, the charge and discharge capacity both increase, with the highest discharge capacity being ca. 140 mA h (g-Sn)$^{-1}$. This increase is explained by the formation of sodium diffusion paths and the enhanced rate of Sn utilization. The highest coulombic efficiency of 95% was recorded in the 3rd cycle. After the 9th cycle, however, there is a rapid decline in both the charge and discharge capacities, indicative of degradation due to the volume change.

The charge–discharge curves for Test No. 3 (cut-off voltages: 0.075 and 0.300 V) are plotted in Fig. 5a. In the first cycle, the charge capacity reaches ca. 500 mA h (g-Sn)$^{-1}$, whereas the discharge capacity is ca. 260 mA h (g-Sn)$^{-1}$. It should be noted that the large difference between the charge and discharge capacity observed in the first cycle is ascribed to charge capacity from plateau (a) given that the first charge was initiated from the rest potential of the Sn-film electrode. The charge–discharge curves for the 2nd and 10th cycles overlap completely in the figure, indicating good cycleability for the initial 10 cycles with a discharge capacity of ca. 250 mA h (g-Sn)$^{-1}$. Fig. 5b shows the cycling properties of the specific capacity and coulombic efficiency from the 1st to the 30th cycles. Although good cycleability is observed until the 10th cycle, both the charge and discharge capacities gradually decrease in the successive cycles, suggestive of electrode degradation. At the 20th

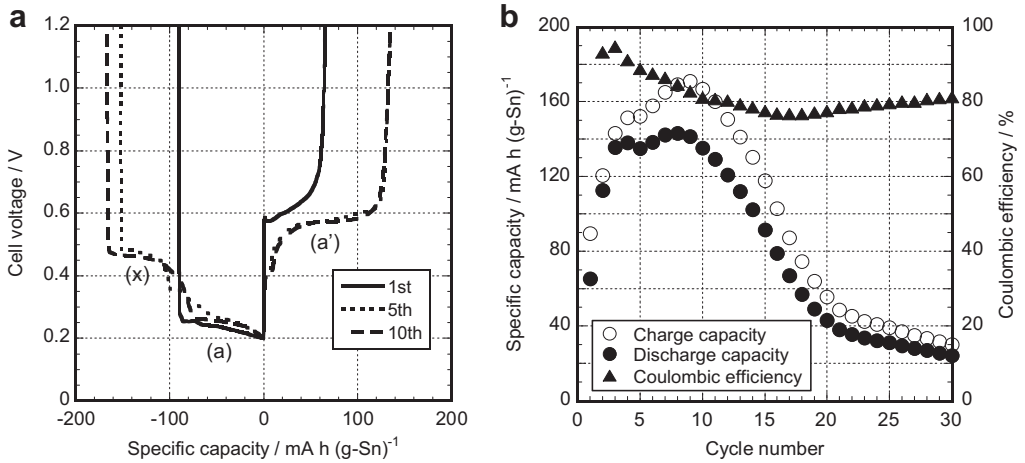

Fig. 4. (a) Charge–discharge curves and (b) cycling properties of specific capacity and coulombic efficiency of the Na/NaFSA–KFSA/Sn cell at 363 K. Cut-off voltages: 0.200 and 1.200 V. Current density: 0.619 mA cm^{-2}.

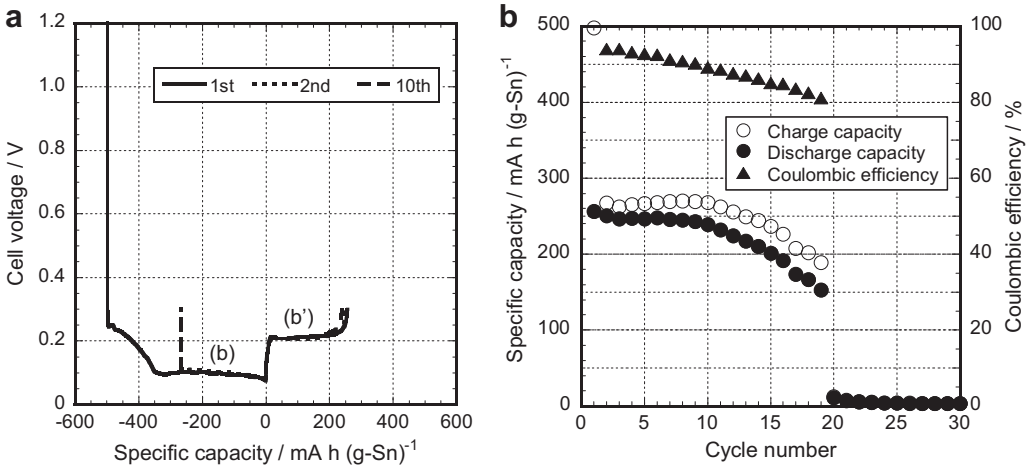

Fig. 5. (a) Charge–discharge curves and (b) cycling properties of specific capacity and coulombic efficiency of the Na/NaFSA–KFSA/Sn cell at 363 K. Cut-off voltages: 0.075 and 0.300 V. Current density: 0.619 mA cm^{-2}.

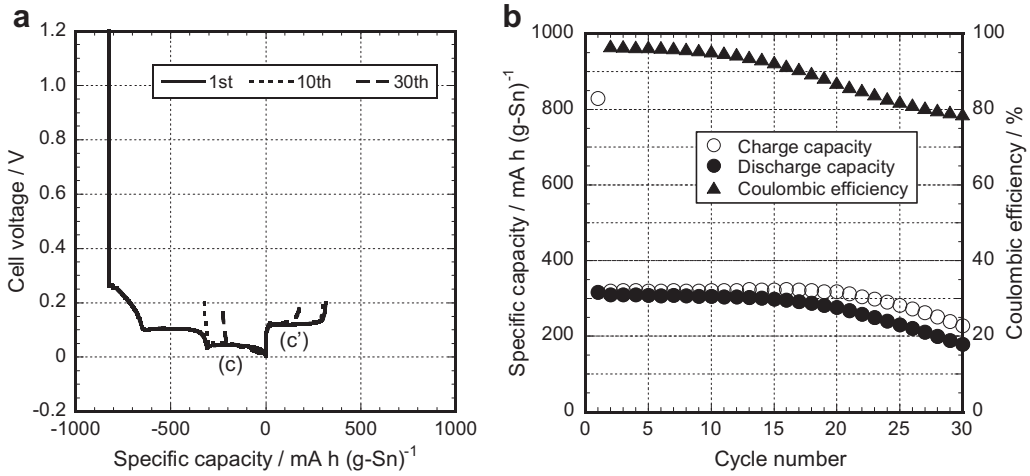

Fig. 6. (a) Charge–discharge curves and (b) cycling properties of specific capacity and coulombic efficiency of the Na/NaFSA–KFSA/Sn cell at 363 K. Cut-off voltages: 0.005 and 0.200 V. Current density: 0.619 mA cm^{-2}.

cycle, there is a precipitous decline in the capacity to less than 20 mA h $(g\text{-}Sn)^{-1}$, which is ascribed to the almost total delamination of the Sn film from the Al-foil substrate [26].

Fig. 6a and b shows the charge–discharge curves and cycling properties of the specific capacity and coulombic efficiency for Test No. 4 (cut-off voltages: 0.005 and 0.200 V). The first charge capacity of ca. 830 mA h $(g\text{-}Sn)^{-1}$ is much larger than the first discharge capacity of ca. 320 mA h $(g\text{-}Sn)^{-1}$. The discrepancy is explained in the same manner as in the case of Test No. 3, with additional capacities corresponding to plateaus (a) and (b). A stable discharge capacity of around 300 mA h $(g\text{-}Sn)^{-1}$ is observed for the initial 15 cycles with a coulombic efficiency higher than 90%. However, the capacity gradually decreased in subsequent cycles to reach ca. 200 mA h $(g\text{-}Sn)^{-1}$ at the 30th cycle, suggesting that the degradation by volume change was not completely suppressed.

The results for Test Nos. 1–4 are compared in Fig. 7 by plotting the discharge capacity against the cycle number. On the basis of both discharge capacity and cycleability, it is clear that a better result is obtained when a lower potential plateau is used. This result is consistent with our hypothesis: the degradation of the Sn negative electrode occurs by volume change, and a smaller volume change gives better cycleability.

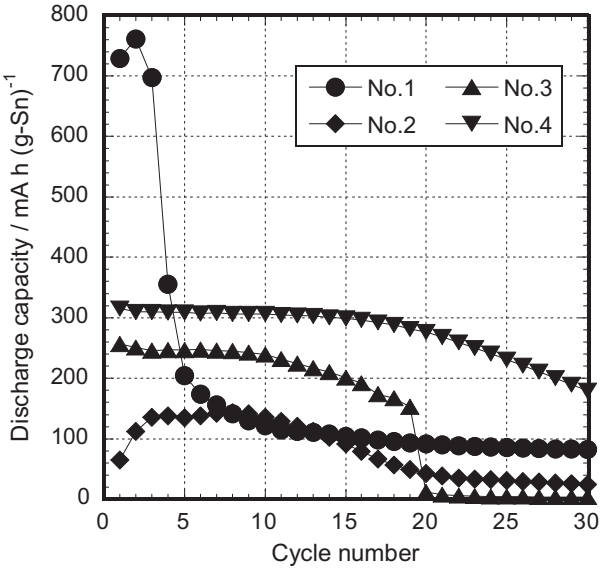

Fig. 7. Summary of discharge capacity of the four charge–discharge tests (Nos. 1–4) stated in Table 2.

4. Conclusions

The charge–discharge behavior of a Sn-film (10–12 μm^t) negative electrode was investigated in the intermediate temperature ionic liquid NaFSA–KFSA at 363 K. The major findings of this study can be summarized as follows:

1. Various Sn–Na alloy phases were formed during the charge–discharge process at 0.619 mA cm^{-2} with cut-off voltages of 0.005 and 1.200 V, evidenced by three potential plateaus in the charge process (a, b, and c) and discharge process (a', b', and c').
2. Based on a comparison of the capacity at each plateau with the theoretical value in the first cycle, the three observed discharge plateaus were tentatively assigned as follows: (a') NaSn/Sn (observed capacity: ca. 200 mA h $(g\text{-}Sn)^{-1}$, theoretical capacity: 226 mA h $(g\text{-}Sn)^{-1}$, volume contraction ratio: 0.45), (b') Na_9Sn_4/NaSn (observed capacity: ca. 250 mA h $(g\text{-}Sn)^{-1}$, theoretical capacity: 282 mA h $(g\text{-}Sn)^{-1}$, volume contraction ratio: 0.63), and (c') $Na_{15}Sn_4/Na_9Sn_4$ (observed capacity: ca. 300 mA h $(g\text{-}Sn)^{-1}$, theoretical capacity: 339 mA h $(g\text{-}Sn)^{-1}$, volume contraction ratio: 0.66) under the afore-stated conditions.
3. The best cycleability is obtained when a lower potential plateau is used, which is consistent with the hypothesis that the degradation of the Sn negative electrode occurs by volume change, and a smaller volume change gives better cycleability.

The results confirmed that Sn is a potential candidate for use as a negative electrode in the sodium secondary battery operating at around 363 K. However, the observed performance in this study, especially the cycleability, is still not sufficient for practical application. As indicated by the results of studies on lithium secondary battery, the use of powdery Sn and Sn alloys will be effective in improving cycle performance.

Acknowledgments

This study was partly supported by Grants-in-Aid for Scientific Research A (No. 20246140) from the Japan Society for the Promotion of Science (JSPS) and by the Advanced Low Carbon Technology

Research and Development Program (ALCA) of Japan Science and Technology Agency (JST).

References

[1] J.L. Sudworth, J. Power Sources 11 (1984) 143–154.
[2] T. Oshima, M. Kajita, A. Okuno, Int. J. Appl. Ceram. Technol. 1 (3) (2004) 269–276.
[3] J. Coetzer, J. Power Sources 18 (1986) 377–380.
[4] C.-H. Dustmann, J. Power Sources 127 (2004) 85–92.
[5] S. Bach, M. Millet, J.P. Periera-Ramos, L. Sanchez, P. Lavela, J.L. Tiradob, Electrochem. Solid-State Lett. 2 (1999) 545–546.
[6] D.A. Stevens, J.R. Dahn, J. Electrochem. Soc. 147 (2000) 1271–1273.
[7] B.L. Ellis, W.R.M. Mskahnouk, Y. Makimura, K. Toghill, L.F. Nazar, Nat. Mater. 6 (2007) 749–753.
[8] I.D. Gocheva, M. Nishijima, T. Doi, S. Okada, J. Yamaki, T. Nishida, J. Power Sources 187 (2009) 247–252.
[9] N. Recham, J.N. Chotard, L. Dupont, K. Djellab, M. Armand, J.M. Tarascon, J. Electrochem. Soc. 156 (2009) A993–A999.
[10] S. Komaba, T. Nakayama, A. Ogata, T. Shimizu, C. Takei, S. Takeda, A. Hokura, N. Nakai, ECS Trans. 16 (42) (2009) 43–55.
[11] S. Komaba, C. Takei, T. Nakayama, A. Ogata, N. Yabuuchi, Electrochem. Commun. 12 (2010) 355–358.
[12] Y. Yamada, T. Doi, I. Tanaka, S. Okada, J. Yamaki, J. Power Sources 196 (2011) 4837–4841.
[13] Y. Kawabe, N. Yabuuchi, M. Kajiyama, N. Fukuhara, T. Inamasu, R. Okuyama, I. Nakai, S. Komaba, Electrochem. Commun. 13 (2011) 1225–1228.
[14] S. Okada, S. Park, Electrochemistry 79 (2011) 470–476 (in Japanese).
[15] R. Hagiwara, K. Tamaki, K. Kubota, T. Goto, T. Nohira, J. Chem. Eng. Data 53 (2008) 355–358.
[16] K. Kubota, K. Tamaki, T. Nohira, T. Goto, R. Hagiwara, Electrochim. Acta 55 (2010) 1113–1119.
[17] K. Kubota, T. Nohira, T. Goto, R. Hagiwara, Electrochem. Commun. 10 (2008) 1886–1888.
[18] K. Kubota, T. Nohira, R. Hagiwara, J. Chem. Eng. Data 55 (2010) 3142–3146.
[19] T. Nohira, T. Ishibashi, R. Hagiwara, J. Power Sources 205 (2012) 506–509.
[20] A. Fukunaga, T. Nohira, Y. Kozawa, R. Hagiwara, S. Sakai, K. Nitta, S. Inazawa, J. Power Sources 209 (2012) 52–56.
[21] S. Komaba, W. Murata, T. Ishikawa, N. Yabuuchi, T. Ozeki, T. Nakayama, A. Ogata, K. Gotoh, K. Fujiwara, Adv. Funct. Mater. 21 (2011) 3859–3867.
[22] S.I. Park, I. Gocheva, S. Okada, J. Yamaki, J. Electrochem. Soc. 158 (2011) A1067–A1070.
[23] P. Senguttuvan, G. Rousse, V. Seznec, J.-M. Tarascon, M.R. Palacín, Chem. Mater. 23 (2011) 4109–4111.
[24] C.M. Park, J.H. Kim, H. Kim, H.J. Sohn, Chem. Soc. Rev. 39 (2010) 3115–3141.
[25] N. Tamura, R. Ohshita, M. Fujimoto, S. Fujitani, M. Kamino, I. Yonezu, J. Power Sources 107 (2002) 48–55.
[26] N. Tamura, R. Ohshita, M. Fujimoto, M. Kamino, S. Fujitani, J. Electrochem. Soc. 150 (2003) A679–A683.
[27] Y. Matsuura, T. Ishikawa, W. Murata, N. Yabuuchi, S. Kuze, S. Komaba, The 52nd Battery Symposium in Japan, Abs. (2011) 182 (in Japanese).
[28] T.B. Massalski, Binary Alloy Phase Diagrams, ASM International, 1990.
[29] F. Dubois, M. Schreyer, T.F. Fässler, Inorg. Chem. 44 (2005) 477–479.
[30] W. Müller, K. Volk, Z. Naturforsch. 32b (1977) 709–710.
[31] W. Müller, K. Volk, Z. Naturforsch. 33b (1978) 275–278.